Hindawi
Mathematical Problems in Engineering
Volume 2019, Article ID 1857931, 13 pages
https://doi.org/10.1155/2019/1857931

Research Article

A Method to Solve the Stiffness of Double-Row Tapered Roller Bearing

Henghai Zhang[1,2] **Wenku Shi**[1] **Guozheng Liu**[1,3] **and Zhiyong Chen**[1]

[1]*State Key Laboratory of Automotive Simulation and Control, Jilin University, Changchun 130022, China*
[2]*School of Automotive Engineering, Shandong Jiaotong University, Jinan 250357, China*
[3]*SAIC Volkswagen Automotive Co., Ltd., Shanghai 201805, China*

Correspondence should be addressed to Zhiyong Chen; chen_zy@jlu.edu.cn

Received 20 February 2019; Revised 11 June 2019; Accepted 8 July 2019; Published 28 July 2019

Academic Editor: José António Fonseca de Oliveira Correia

By analyzing the roller force, the nonlinear stiffness model of the double-row tapered roller hub bearing is derived, and the method of solving the hub bearing stiffness matrix is summarized: if the displacement between the inner and outer rings is known, the stiffness of the hub bearing can be directly calculated. If only the external load of the hub bearing is known, the displacement of the hub bearing needs to be solved by numerical method, and then the stiffness of the hub bearing can be calculated. The improved Newton-Raphson method is used to solve the stiffness matrix of the hub bearing. Three-dimensional FE model of DRTRBs is presented and validated the proposed the stiffness matrix of the hub bearing. It is found that the radial stiffness of the hub bearing is greater than the axial stiffness. The stiffness of the hub bearing is greatly affected by the vertical force of the ground and the wheel driving torque, showing obvious nonlinearity. The smaller the vertical ground load and wheel driving torque, the greater the influence of vertical ground load and wheel driving torque on the hub bearing stiffness.

1. Introduction

Double-row Tapered Roller Bearings (DRTRBs) are designed to support the preload, axial load, radial load, and torque in static and dynamic conditions [1, 2]. DRTRBs have been particularly considered in high-load supporting applications in automobile wheel hub assembly. Stiffness is the essential factors that significantly affect the performance of DRTRBs; bearing stiffness is needed for analyzing the dynamic characteristics, for example, natural frequencies, mode shapes, and vibration amplitudes [3–10].

The first few major works on rolling element bearing stiffness were performed by Palmgren [11], Jones [12], Dowson [13], and Harris [14], which were adopted in numerous bearing analyses [8, 15–18]. De Mul et al. [17, 18] computed analytically the bearing stiffness matrix of roller bearings based on the theory of Jones [12] and used internally in the iterative bearing equilibrium calculation. Tong and Hong [4, 19] presented time-varying stiffness matrix of tapered roller bearings (TRBs) based on the bearing stiffness matrix based on the theory of De Mul et al. [17, 18]. Based on the Hertzian theory, Lim et al. [3, 9, 10] derivated a time invariant bearing stiffness matrix of dimension 5. Kabus et al. [20] presented a new multidegree of freedom frictionless quasi-static time-domain TRBs model which allows for an arbitrary stiffness of the outer ring supporting structure. In a CAD environment, Bourdon et al. [21] developed an alternative method to estimate the stiffness matrix and discussed the influence of the static loads on the stiffness matrices of TRBs in a rigid environment. Guo and Parker [22] developed a finite element contact mechanics model and obtained accurate bearing stiffness for a wide range of bearing types (cylindrical and ball bearings) and parameters, and the stiffness matrix is calculated numerically through finite differences to first, second, fourth, and sixth order, respectively. However, the research papers did not covered the stiffness derivation of DRTRBs.

Though DRTRBs are widely used in industrial, the study on stiffness derivation of DRTRBs is sparse. For instance, Gunduz et al. [23] computed stiffness matrix for double-row angular contact ball bearings. However, inertial loading due to the rotational speed effect was not considered in

(a) Back-to-back arrangement (b) Face-to-face arrangement

Figure 1: Double-row tapered roller bearing.

their bearing model. Bercea et al. [24, 25] presented the relationship of bearing stiffness given by Harris [14] in a DRTRBs example, and formulated the relative displacement between the bearing rings for various double-row bearing types such as DRTRBs [26]. Fernandez et al. [2] optimized presetting loads to improve working conditions for a double-row TRB. In many static and dynamic problems, a double-row bearing must be considered as an integrated unit. The stiffness matrices of two single-row bearings may not be simply superposed to obtain the stiffness matrix of DRTRBs [23]. So the stiffness of DRTRBs is derived.

To overcome the deficiency in the literature, an approach about stiffness for DRTRBs is proposed based on the Hertzian theory for back-to-back arrangements. By analyzing the roller force, the nonlinear stiffness model of the double-row tapered roller hub bearing is derived. Then the improved Newton-Raphson method is used to solve the stiffness matrix of the hub bearing. The proposed stiffness model was validated by a proposed finite element model of double-row tapered roller hub bearing.

2. Structure of Hub Bearing

The hub bearing studied in this paper is DRTRBs that support the semifloating drive axle. The axle housing is a steel plate stamping and welding structure. There are six bearings in the drive axle; four single-row tapered roller bearings (SRTRBs) in the final reduction drive and two DRTRBs are hub bearing.

As shown in Figure 1, DRTRBs are often arranged in a back-to-back or face-to-face arrangement generally. The DRTRBs studied in this paper are installed in a back-to-back arrangement. Generally, DRTRBs are formed by a pair of inner raceways that are separated by a gap of constant distance, an outer raceway, and a group of tapered rollers that are located between the inner and outer raceways. The stiffness calculation method of DRTRBs is different from that of SRTRBs.

3. Nonlinear Stiffness Model of Hub Bearing

3.1. Contact Deformations. The difficulty is to calculate contact mechanical properties between roller and inner and outer ring of bearing. To solve this problem, the elastic deformation and stress distribution of the contact surface should be analyzed firstly. Hertz's elastic contact theory [27] and Sjovall's integrals [28] is the basis for predicting the stiffness of rolling bearings. Hertz's theory makes the following assumptions:

(1) The contact body is an isotropic linear elastic material, which obeys Hooke's law and is in a small deformation state.

(2) The length a of the contact area is much smaller than the radius R of curvature of the surface of the object, that is, $a \ll R$.

(3) The contact surface is smooth and continuous, and there is no friction.

(4) Since $a \ll R$, every object can be regarded as an elastic half space.

For the elastic deformation of the line contact problem, there is generally no accurate analytical solution, and an empirical formula or an approximate formula is usually used. Palmgren [11] proposed an empirical formula for the linear contact elastic deformation, expressed by the relation

$$\delta = 3.84 \times 10^{-5} \frac{Q^{0.9}}{l^{0.8}} \tag{1}$$

where δ denotes the elastic deformation of bearing roller, Q denotes the normal load in the contact area of the roller, and l describes the length of the roller. Equation (1) shows that the roller deformation is independent of the curvature radius of the roller and inner and outer ring and only depends on the roller length and the normal load, so the elastic deformation of bearing roller is only an approximation. When the diameter of the bearing roller and the bearing ring changes, the elastic deformation of bearing roller does not change, and sometimes it differs greatly from the true value.

Houpert [29] proposed an empirical formula for the elastic deformation, which can be described as

$$Q = 6.39 \times 10^{10} l^{0.991} D^{0.1034} \delta^{1.1} \tag{2}$$

Ding Chang'an [30] proposed an analytical solution to elastic line contact of finite length, taking into account the

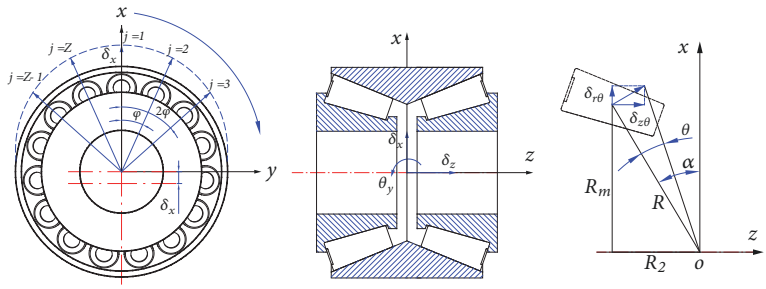

Figure 2: Relation between bearing load and displacement.

curvature radius of the contact surface; the elastic deformation can be expressed by

$$\delta = \frac{\eta Q}{\pi l} \ln \frac{6.95 l^3 (R_1 \pm R_2)}{\eta Q R_1 R_2} \tag{3}$$

To calculate the stiffness of the rolling bearing, Wu Hao [31] proposed that the elastic deformation formula is expressed as

$$\delta = \frac{2Q}{\pi l} \frac{1 - v^2}{E} \left(\ln \frac{4R_1 R_2}{b^2} + 0.814 \right) \tag{4}$$

Luo Jiwei [32] verified the Palmgren's empirical formula (1) and calculated the elastic deformation of the cylindrical roller with l=10mm when it was in contact with the half plane. The result shows that the elastic deformation is correct only when the radius of cylindrical roller is 20 mm, and the elastic deformation will change greatly when the radius of the roller changes. Considering the diameter of the bearing roller and the inner and outer rings of the bearing, Luo Jiwei proposed the modified Palmgren formula, which can be described as

$$\delta = 4.83 \times 10^{-5} \frac{Q^{0.9}}{D_W{}^{0.1} l^{0.74}} (1 \pm k)^{0.1} \tag{5}$$

where δ denotes the elastic deformation of rollers. D_W and l denote the diameter and length of the roller, respectively. Q denotes the normal load in the contact zone of roller. D_r denotes the diameter of the raceway. Considering the unevenness of the curvature of the contact surface, "+" denotes that the roller is in contact with the inner ring, and "-" denotes that the roller is in contact with the outer ring.

Based on the modified Palmgren formula, the force and stiffness model of tapered roller bearings is derived. The stiffness between the roller and the inner and outer rings is k_i and k_e, respectively. The elastic contact deformation between roller and inner and outer rings is δ_{Ei} and δ_{Ee}, respectively. The elastic contact deformation between roller and inner and outer rings can be interpreted as two springs in series [20]. Because the taper angle of the tapered roller is small, for the sake of simplicity of calculation, it is treated as a cylindrical roller. D_W is the average diameter of the tapered roller. According to (5), the contact deformation between roller and inner and outer rings can be expressed by

$$\delta_{Ei} = 4.83 \times 10^{-5} \frac{Q_i^{0.9}}{D_W{}^{0.1} l^{0.74}} (1 + k)^{0.1} \tag{6}$$

$$\delta_{Ee} = 4.83 \times 10^{-5} \frac{Q_e^{0.9}}{D_W{}^{0.1} l^{0.74}} (1 - k)^{0.1} \tag{7}$$

The contact deformation between the inner ring and the roller is projected to the direction of the contact force of the outer ring with the reference of the contact deformation of the outer ring of the bearing. The projection of δ_{Ei} in Q_e direction is $\delta_{Ei} \cos \beta$, so the total relative displacement of the inner and outer rings of the bearing in the Q_e direction,

$$\delta_n = \delta_{Ee} + \delta_{Ei} \cos \beta \tag{8}$$

where β denotes the cone angle of the roller. Substituting (6) and (7) into (8), the total relative displacement can be expressed by

$$\delta_n = 4.83 \times 10^{-5} \frac{Q_e^{0.9}}{D_W{}^{0.1} l^{0.74}} \left[(1 - k)^{0.1} + (1 + k)^{0.1} \cos \beta \right] \tag{9}$$

3.2. Bearing Force. As shown in Figure 2, the geometric center of the bearing is the coordinate origin O. The distance from the center of the roller to the origin of the coordinate is R. The projections of R in the radial and axial directions are R_m and R_2, respectively.

Referring to the stiffness analysis of SRTRBs, assuming that the outer ring of the bearing is fixed, the inner ring and the roller are taken as a whole. The deformation and force of the left rollers and the right rollers are analyzed, respectively.

3.2.1. Force Induced the Left-Hand Rollers. For the displacement components δ_r, the axial displacement δ_z, and the rotation angle θ of the inner ring relative to the outer ring, the radial displacement of the jth roller on the left side of the bearing (azimuth angle φ_j) due to rotation angle θ is expressed by

$$\delta_{r\theta j} = R\theta \cos \varphi_j \sin \alpha = R_2 \theta \cos \varphi_j \tag{10}$$

The total radial displacement of the jth roller on the left-hand bearings can be expressed by

$$\delta_{rj} = \delta_r \cos\varphi_j + \delta_{r\theta j} = (\delta_r + R_2\theta)\cos\varphi_j \tag{11}$$

The axial displacement of the jth roller on the left-hand bearings (azimuth angle φ_j) due to rotation angle θ is expressed by

$$\delta_{z\theta j} = R\theta\cos\varphi_j\cos\alpha = R_m\theta\cos\varphi_j \tag{12}$$

The total axial displacement of the jth roller on the left-hand bearings can be expressed by

$$\delta_{zj} = \delta_z + \delta_{z\theta j} = \delta_z + R_m\theta\cos\varphi_j \tag{13}$$

Since the radial displacement δ_r includes displacements δ_x and δ_y along x axis and y axis, the rotation angle θ includes rotation angles θ_x and θ_y around x axis and y axis, The total radial displacement and axial displacement of the jth roller on the left-hand bearings can be expressed by

$$\begin{aligned}\delta_{r1j} &= \left(\delta_x\cos\varphi_j + \delta_y\sin\varphi_j\right) \\ &\quad + R_2\left(\theta_x\sin\varphi_j - \theta_y\cos\varphi_j\right) \\ \delta_{z1j} &= \delta_z + R_m\left(\theta_x\sin\varphi_j - \theta_y\cos\varphi_j\right)\end{aligned} \tag{14}$$

The additional moment caused by the axial component of the roller contact force can be expressed by

$$\begin{aligned}M_{ax1} &= \sum_{j=1}^{Z}\left[R_m\sin\varphi_j Q_{e1j}\sin\alpha_e\right] \\ M_{ay1} &= -\sum_{j=1}^{Z}\left[R_m\cos\varphi_j Q_{e1j}\sin\alpha_e\right]\end{aligned} \tag{15}$$

The additional moment caused by the radial component of the roller contact force can be expressed by

$$\begin{aligned}M_{rx1} &= \sum_{j=1}^{Z}\left[R_2\sin\varphi_j Q_{e1j}\cos\alpha_e\right] \\ M_{ry1} &= -\sum_{j=1}^{Z}\left[R_2\cos\varphi_j Q_{e1j}\cos\alpha_e\right]\end{aligned} \tag{16}$$

The directions of force and displacement refer to the coordinate system in Figure 2, and the directions of rotation and torque obey the right-hand rule. The bearing forces and moments induced by the left-hand rollers can be expressed by

$$\begin{aligned}F_{x1} &= \sum_{j=1}^{Z}\left[Q_{e1j}\cos\alpha_e\cos\varphi_j\right] \\ F_{y1} &= \sum_{j=1}^{Z}\left[Q_{e1j}\cos\alpha_e\sin\varphi_j\right] \\ F_{z1} &= \sum_{j=1}^{Z}\left[Q_{e1j}\sin\alpha_e\right] \\ M_{x1} &= \left(R_2\cos\alpha_e + R_m\sin\alpha_e\right)\sum_{j=1}^{Z}\left[Q_{e1j}\sin\varphi_j\right] \\ M_{y1} &= -\left(R_2\cos\alpha_e + R_m\sin\alpha_e\right)\sum_{j=1}^{Z}\left[Q_{e1j}\cos\varphi_j\right] \\ M_{z1} &= 0\end{aligned} \tag{17}$$

3.2.2. Force Induced the Right-Hand Rollers. The above analysis is only for the left-hand rollers. The forces on the left-hand rollers and the right-hand rollers are different. The absolute value of the displacement and load of each roller on the right side is the same as the corresponding left roller, but the directions are not exactly the same. For example, when the inner ring is subjected to the axial displacement δ_z, the left-hand roller is close to the outer ring, and the right-hand roller is away from the outer ring. Then the contact force between the left-hand roller and the outer ring increases, while the contact force between the right-hand roller and the outer ring decreases. Referring to the force analysis of the left roller, the radial and axial displacements of the jth roller on the right can be expressed by

$$\begin{aligned}\delta_{r2j} &= \left(\delta_x\cos\varphi_j + \delta_y\sin\varphi_j\right) \\ &\quad - R_2\left(\theta_x\sin\varphi_j - \theta_y\cos\varphi_j\right) \\ \delta_{z2j} &= -\delta_z - R_m\left(\theta_x\sin\varphi_j - \theta_y\cos\varphi_j\right)\end{aligned} \tag{18}$$

The bearing forces and moments induced by the right-hand rollers can be expressed by

$$\begin{aligned}F_{x2} &= \sum_{j=1}^{Z}\left[Q_{e2j}\cos\alpha_e\cos\varphi_j\right] \\ F_{y2} &= \sum_{j=1}^{Z}\left[Q_{e2j}\cos\alpha_e\sin\varphi_j\right] \\ F_{z2} &= -\sum_{j=1}^{Z}\left[Q_{e2j}\sin\alpha_e\right] \\ M_{x2} &= -\left(R_2\cos\alpha_e + R_m\sin\alpha_e\right)\sum_{j=1}^{Z}\left[Q_{e2j}\sin\varphi_j\right] \\ M_{y2} &= \left(R_2\cos\alpha_e + R_m\sin\alpha_e\right)\sum_{j=1}^{Z}\left[Q_{e2j}\cos\varphi_j\right] \\ M_{z2} &= 0\end{aligned} \tag{19}$$

3.2.3. Bearing Force and Moments. According to (17) and (19), the force and moment in all directions of the double-row roller bearing can be expressed by

$$F_x = \sum_{j=1}^{Z}\left[\left(Q_{e1j} + Q_{e2j}\right)\cos\alpha_e\cos\varphi_j\right]$$

$$
\begin{aligned}
F_y &= \sum_{j=1}^{Z}\left[\left(Q_{e1j}+Q_{e2j}\right)\cos\alpha_e\sin\varphi_j\right]\\
F_z &= \sum_{j=1}^{Z}\left[\left(Q_{e1j}-Q_{e2j}\right)\sin\alpha_e\right]\\
M_x &= \left(R_m\sin\alpha_e+R_2\cos\alpha_e\right)\sum_{j=1}^{Z}\left(Q_{e1j}-Q_{e2j}\right)\sin\varphi_j\\
M_y &= \left(R_m\sin\alpha_e+R_2\cos\alpha_e\right)\sum_{j=1}^{Z}\left(Q_{e2j}-Q_{e1j}\right)\cos\varphi_j\\
M_z &= 0
\end{aligned}
\tag{20}
$$

where Q_{e1j} and Q_{e2j} are the normal loads of the jth roller on the left-hand bearings and the right-hand bearings, respectively. According to (9), (14), and (18), the normal displacement of each roller can be expressed by

$$
\begin{aligned}
\delta_{nij} = &\left[\left(\delta_x\cos\varphi_j+\delta_y\sin\varphi_j\right)\right.\\
&-(-1)^i R_2\left(\theta_x\sin\varphi_j-\theta_y\cos\varphi_j\right)\left.\right]\cos\alpha_e-(-1)^i\\
&\cdot\left[\delta_z+R_m\left(\theta_x\sin\varphi_j-\theta_y\cos\varphi_j\right)\right]\sin\alpha_e
\end{aligned}
\tag{21}
$$

Substituting (21) into (9), the normal load between each roller and the outer ring can be expressed by

$$
Q_{eij}=\begin{cases}K_{ne}{\delta_{nij}}^{1.11} & \left(\delta_{nij}>0\right)\\ 0 & \left(\delta_{nij}\le 0\right)\end{cases}
\tag{22}
$$

In (21) and (22), the directions of force and displacement refer to the coordinate system in Figure 2, and the directions of rotation and moments obey the right-hand rule. When the outer ring is fixed and the inner ring is subjected to force F_i ($i = x, y, z$) and moments M_i ($i = x, y, z$), the displacement and rotation angles of the inner ring are δ_i ($i = x, y, z$) and θ_i ($i = x, y, z$), respectively.

4. Solution of Hub Bearing Stiffness Matrix

4.1. Bearing Stiffness Matrix. Bearings are often simplified to spring elements with axial and radial stiffness in the finite element modeling of drive axle assembly. In fact, the bearing has five directions of stiffness except for the degree of freedom around the z axis, and the stiffness in each direction is coupled. Therefore, the bearing stiffness matrix can be more accurately expressed by

$$
K=\begin{bmatrix}
\frac{\partial F_x}{\partial\delta_x} & \frac{\partial F_x}{\partial\delta_y} & \frac{\partial F_x}{\partial\delta_z} & \frac{\partial F_x}{\partial\theta_x} & \frac{\partial F_x}{\partial\theta_y} & 0\\
\frac{\partial F_y}{\partial\delta_x} & \frac{\partial F_y}{\partial\delta_y} & \frac{\partial F_y}{\partial\delta_z} & \frac{\partial F_y}{\partial\theta_x} & \frac{\partial F_y}{\partial\theta_y} & 0\\
\frac{\partial F_z}{\partial\delta_x} & \frac{\partial F_z}{\partial\delta_y} & \frac{\partial F_z}{\partial\delta_z} & \frac{\partial F_z}{\partial\theta_x} & \frac{\partial F_z}{\partial\theta_y} & 0\\
\frac{\partial M_x}{\partial\delta_x} & \frac{\partial M_x}{\partial\delta_y} & \frac{\partial M_x}{\partial\delta_z} & \frac{\partial M_x}{\partial\theta_x} & \frac{\partial M_x}{\partial\theta_y} & 0\\
\frac{\partial M_y}{\partial\delta_x} & \frac{\partial M_y}{\partial\delta_y} & \frac{\partial M_y}{\partial\delta_z} & \frac{\partial M_y}{\partial\theta_x} & \frac{\partial M_y}{\partial\theta_y} & 0\\
0 & 0 & 0 & 0 & 0 & 0
\end{bmatrix}
\tag{23}
$$

Diagonal terms in the stiffness matrix include radial stiffness $\partial F_i/\partial\delta_i$, axial stiffness $\partial F_z/\partial\delta_z$, and angular stiffness $\partial M_i/\partial\theta_i$, where i=x, y. The off-diagonal cross-coupling terms in the stiffness matrix are the coupling stiffness values. The local coordinate system of the bearing is shown in Figure 2. The bearing is free to rotate about the z axis, so the sixth row and column in the stiffness matrix are zero. The stiffness matrix is symmetric because the bearing system is conservative. The load and displacement equations of bearings can be expressed by

$$
P_b = K\delta_b
\tag{24}
$$

where load vector is $P_b = [F_x, F_y, F_z, M_x, M_y, M_z]^T$ and displacement vector is $\delta_b = [\delta_x, \delta_y, \delta_z, \theta_x, \theta_y, \theta_z]^T$.

4.2. Force on Hub Bearing. Hub bearings studied in this paper are DRTRBs. The structure of the left and right hub bearings and the applied load are exactly the same. DRTRBs support the semifloating drive axle as shown in Figure 3. That is, the rear drive shaft is subjected to the moments transmitted from the vehicle transmission system and the vertical load of the wheel. The bearing is subjected to vertical and driving force from the road, as well as the bending moments induced by them.

To coincide with the coordinate system shown in Figure 2, the vertical force and the driving force of the road surface are represented by F_z and F_x, respectively. The force and moments of the hub bearing can be expressed by

$$
\begin{aligned}
F_x &= \frac{G_r}{2}\\
F_y &= \frac{T_r}{r_0}\\
F_z &= 0\\
M_x &= \frac{T_r b}{r_0}\\
M_y &= \frac{G_r b}{2}
\end{aligned}
\tag{25}
$$

where G_r denotes the rear axle load. T_r denotes the wheel driving torque. r denotes the tire rolling radius. b denotes the distance from the center of the wheel to the center of the hub bearing.

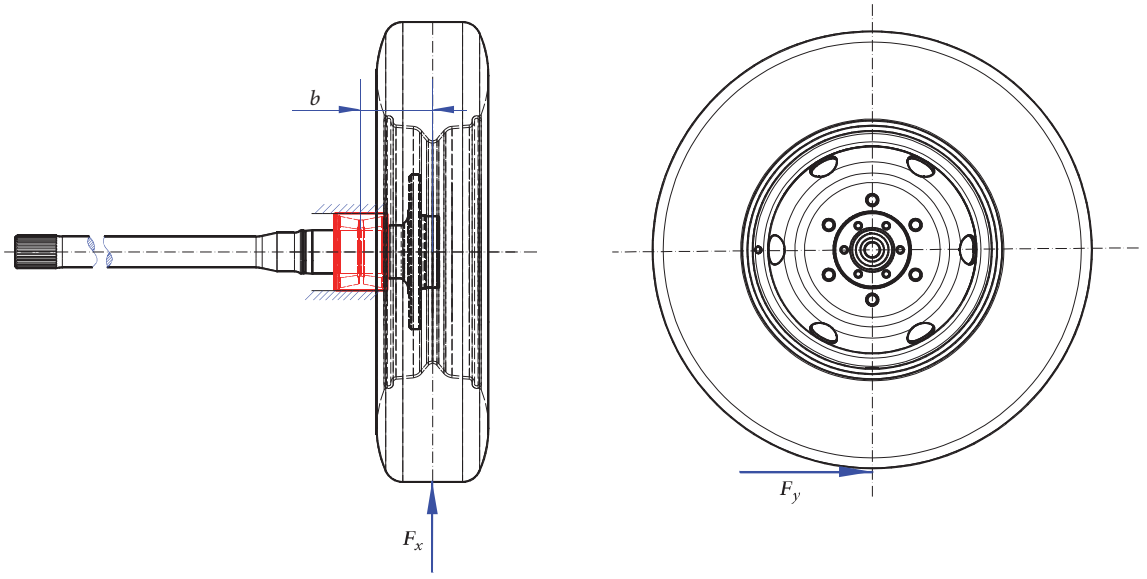

Figure 3: Hub bearing relationship load vs. displacement.

4.3. Solution of Stiffness Matrix. The stress of hub bearing is relatively simple, so it is not necessary to adopt the method of finite element iteration. According to the external loads on the bearing, the displacement δ_i and the rotation angle θ_i between the inner and outer rings of the bearing are obtained. Then, the stiffness value of the bearing can be calculated by substituting δ_i and θ_i into (23).

According to (20) and (25), the relation of the displacement and rotation angle between inner and outer rings under external loads can be expressed by

$$\begin{aligned}
f_1 &= \sum_{j=1}^{Z}\left[\left(Q_{e1j}+Q_{e2j}\right)\cos\alpha_e\cos\varphi_j\right]-F_x=0\\
f_2 &= \sum_{j=1}^{Z}\left[\left(Q_{e1j}+Q_{e2j}\right)\cos\alpha_e\sin\varphi_j\right]-F_y=0\\
f_3 &= \sum_{j=1}^{Z}\left[\left(Q_{e1j}-Q_{e2j}\right)\sin\alpha_e\right]-F_z=0\\
f_4 &= \left(R_m\sin\alpha_e+R_2\cos\alpha_e\right)\\
&\quad\cdot\sum_{j=1}^{Z}\left(Q_{e1j}-Q_{e2j}\right)\sin\varphi_j-M_x=0\\
f_5 &= \left(R_m\sin\alpha_e+R_2\cos\alpha_e\right)\\
&\quad\cdot\sum_{j=1}^{Z}\left(Q_{e2j}-Q_{e1j}\right)\cos\varphi_j-M_y=0
\end{aligned}\tag{26}$$

where $F=[f_1,f_2,f_3,f_4,f_5]^T$, external Loads Vector $P_b=[F_x,F_y,F_z,M_x,M_y]^T$, displacement vector $X=[\delta_x,\delta_y,\delta_z,\theta_x,\theta_y]^T$, bearing stiffness matrix is $K(5\times5)$, and then (26) can be expressed by

$$F=KX-P\tag{27}$$

Equation (26) is a set of nonlinear equations for five variables δ_x,δ_y,δ_z, θ_x, and θ_y. It is almost impossible to solve the exact solution by analytical method. In this paper, the improved Newton iteration method is used to solve this problem.

Newton-Raphson method is also called the tangent method. By continuously making the tangent of the curve $y=f(x)$ and finding the coordinates of the intersection of the curve and the x axis, the solution of the equation $f(x)=0$ can be obtained. The iterative formula of the one-dimensional equation can be expressed by

$$x_{k+1}=x_k-\frac{f(x_k)}{f'(x_k)}\tag{28}$$

In (28), the selection of initial value x_0 will have a great impact on the convergence of the algorithm. This paper uses the improved Newton-Raphson method to calculate the displacement and stiffness of the hub bearing. The improved Newton-Raphson method of the one-dimensional equation can be expressed by

$$x_{k+1}=x_k-\frac{f\left[x_k-f(x_k)/f'(x_0)\right]}{f'\left[x_k-f(x_k)/f'(x_0)\right]}\tag{29}$$

For multidimensional equations, the improved Newton-Raphson method can be expressed by

$$\begin{aligned}
-\boldsymbol{K}(\boldsymbol{X}_0)\Delta\boldsymbol{X}_k&=\boldsymbol{F}(\boldsymbol{X}_k)\\
\widetilde{\boldsymbol{X}}_k&=\boldsymbol{X}_k+\Delta\boldsymbol{X}_k\\
-\boldsymbol{K}\left(\widetilde{\boldsymbol{X}}_k\right)\Delta\widetilde{\boldsymbol{X}}_k&=\boldsymbol{F}(\boldsymbol{X}_k)\\
\boldsymbol{X}_{k+1}&=\boldsymbol{X}_k+\Delta\widetilde{\boldsymbol{X}}_k
\end{aligned}\tag{30}$$

It can be seen from (30) that the improved Newton-Raphson method divides the iteration process into two

Table 1: Material parameters of DRTRBs.

Density	P($tonne/mm^3$)	7.85×10^{-9}
Young's modulus	E (N/mm^2)	2.06×10^5
Poisson's ratio	ν	0.3

steps. Firstly, the intermediate variable $\widetilde{X_k}$ is obtained by evaluating X_k. Secondly, $\widetilde{X_k}$ is substituted into Newton-Raphson method, which can reduce the influence of initial value deviation on convergence. In order to improve the convergence, combined with Newton downhill method, the iterative formula can be expressed by

$$X_{k+1} = X_k + \lambda\Delta\widetilde{X_k} \tag{31}$$

where λ ($0 < \lambda < 1$) is the downhill parameter or relaxation factor. The downhill condition can be expressed by

$$\left|F\left(X_{k+1}\right)\right| < \left|F\left(X_k\right)\right| \tag{32}$$

The downhill condition is satisfied by adjusting the magnitude of λ adaptively. When the downhill condition is satisfied, it is the classical Newton iteration method. When the downhill condition is not satisfied, λ is reduced by half until the downhill condition is satisfied. The calculation process of hub bearing displacement and rotation angle based on the improved Newton-Raphson method is shown in Figure 4.

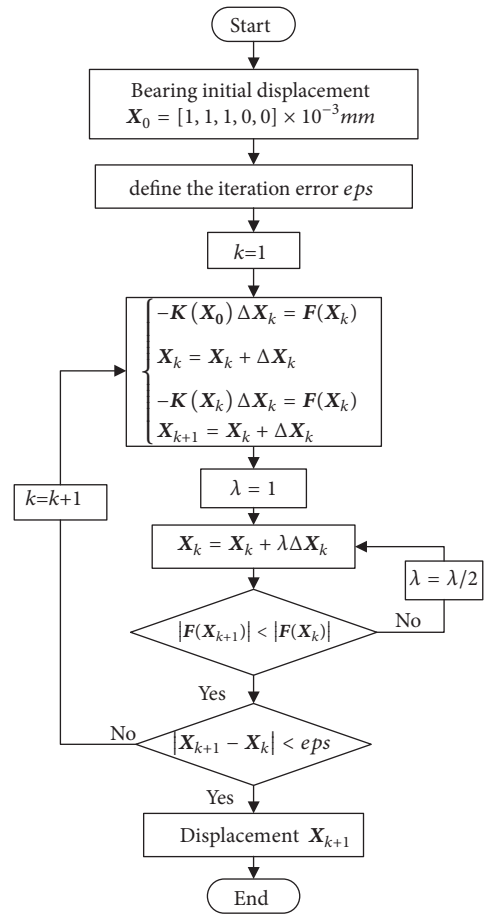

Figure 4: Calculation flowchart for hub bearing.

5. Finite Element Model Validation

A numeric model of the ball bearing is established using ABAQUS [33, 34]. In order to validate the method of bearing stiffness, three-dimensional FE model of DRTRBs is presented using ABAQUS, which is shown in Figure 5. Because of the nonlinearity of mechanical contact in the use of FEM, contact stresses are unrealistic when the FE models have limited contact surface and the size of mesh is very large. This problem is usually solved by making the mesh between contact pairs small, i.e., increasing the number of contact nodes. Demirhan and Kanber studied the effect of FE model element size on contact stress between the raceway and rollers [35]. Fernandez et al. used small mesh size to obtain fine FE models with contact areas. By using small mesh sizes of contact areas, the contact stress obtained by finite element method is not much different from that by theoretical analysis and experimental method [2]. Considering the central processing unit (CPU) running time increases exponentially with the element dimension decreases, mesh refinement on the contact areas of the rollers shown in Figure 6 was applied. To ensure high computation accuracy of contact stresses, the finite-element mesh is generated C3D8R elements, and the total number of elements is 1,757,080 using Hypermesh software. Raceways and tapered rollers are modeled using linear elastic and isotropic steel. The geometry and material parameters of the roller bearing are given in Tables 1 and 2.

The outer surface of the outer raceway is developed as fixed surface and static radial force was applied in the center of the bearing. A reference point is established in the center of rotation of the inner ring, the part of the inner surface of inner ring is coupled with the reference point. The interaction between surfaces is defined as surface-to-surface contact with no adjustment. Interaction properties are imposed using surface-to-surface hard normal contact between the master surface of roller and the slave surface of the outer raceway as well as between the master surface of roller and the slave surface of the inner raceway. The coefficient between the rollers and the inner raceway and between the rollers and the outer raceway is 0.001 [35].

The bearing stress distribution of FEM can be obtained when the radial force was applied. Figure 7 shows the stresses distribution on the outer raceway and inner raceway caused by the first and second row of rollers, which is in good agreement with the stresses distribution studied by

Table 2: Geometrical parameters of double-row tapered roller hub bearings.

Parameters	Symbol	Value
Roller length	$L\ (mm)$	20
Roller mean diameter	$r\ (mm)$	5
Number of rollers in one row	Z	15
Pitch diameter	$R_m\ (mm)$	60
Distance between Bearing Center and Roller Center	$R\ (mm)$	68
Inner diameter	$D_i\ (mm)$	50
Outer diameter	$D_e\ (mm)$	70

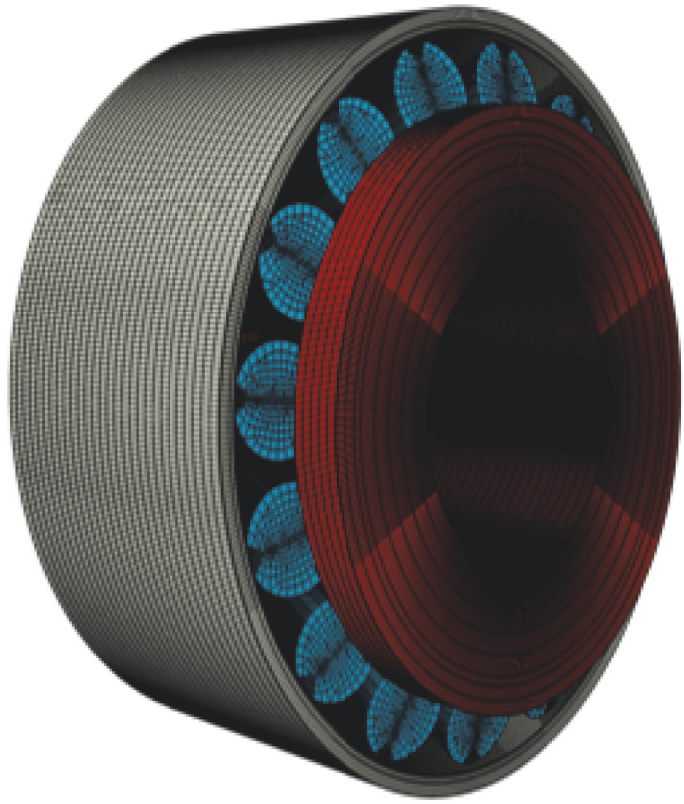

Figure 5: FE model configuration.

Harris [36] and Lostado et al. [1] for DRTRBs. Figure 8 shows the variation of the radial force and the radial stiffness with respect to radial displacement of the bearing. Figure 9 shows variation of the moment and the tilting stiffness with respect to angular displacement of the bearing; Figures 8 and 9 are in good agreement with the load-deflection relationship that was studied by Harris [36] and Kania [37] for DRTRBs. The largest error shown on the Figures 8 and 9 is less than 10%. FEM verification of the proposed stiffness model is available.

6. Results and Discussions

When the rear axle is fully loaded with 16kN and the drive torque is 200Nm. The relevant dimensions of the chosen hub bearing are listed in Table 2. The hub bearing displacement vector is obtained by the above method, $X = [7.742mm, 0.067mm, 20.62mm, 0.0099rad, 0.2405rad]^T \times 10^{-3}$. The five-dimensional stiffness matrix of hub bearing can be obtained by (20), (21), and (23). The stiffness matrix of hub bearing is expressed by

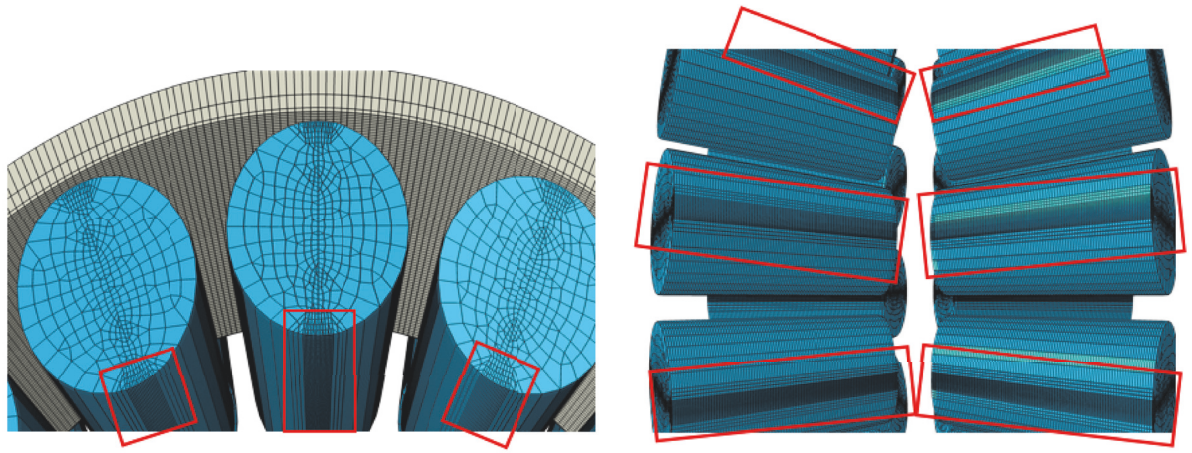

(a) Between the rollers and the inner raceway (b) Between the rollers and the outer raceway

Figure 6: Contact areas of the rollers.

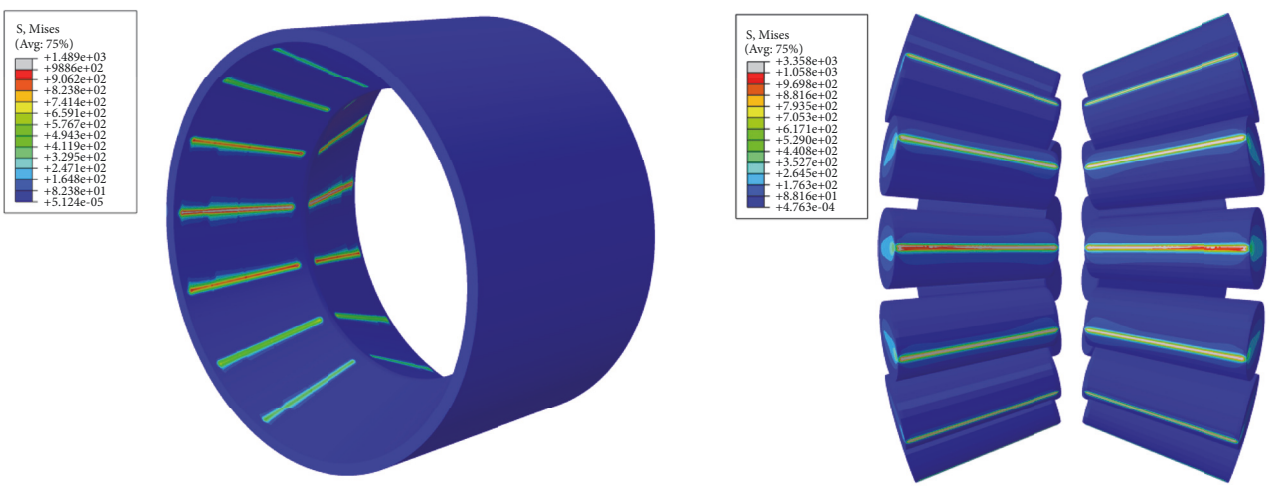

(a) The outer raceway (b) The rollers

Figure 7: The stresses distribution on the outer raceway and the rollers.

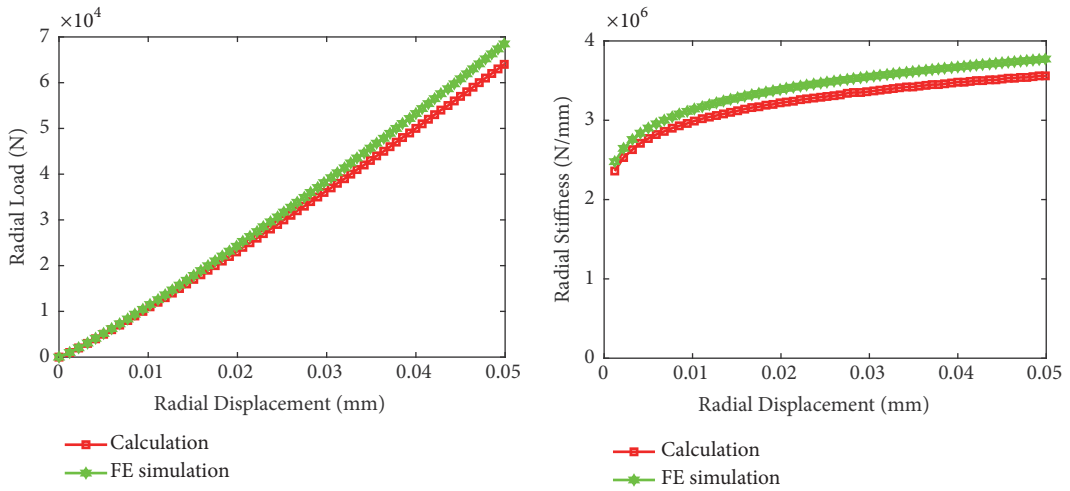

Figure 8: Variation of the radial force and the radial stiffness with respect to radial displacement of the bearing.

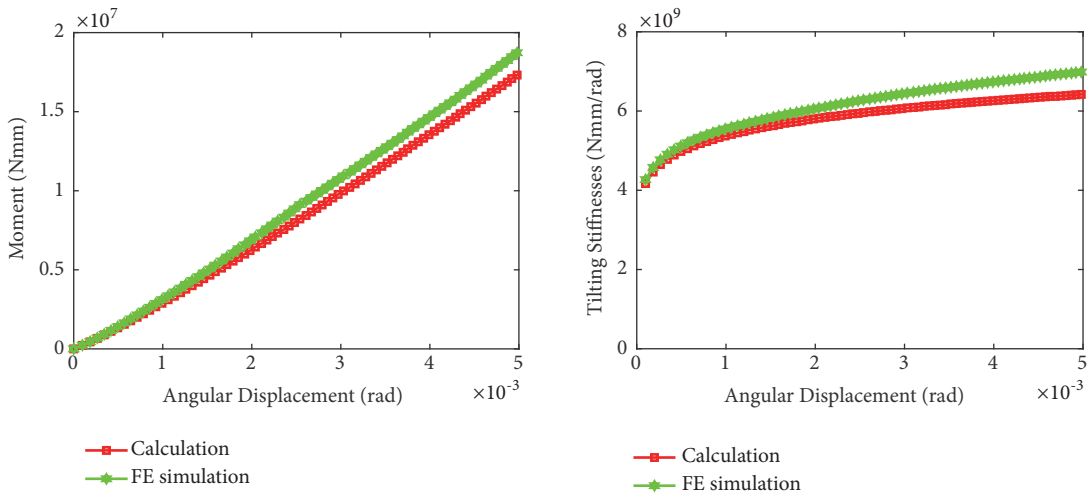

Figure 9: Variation of the moment and the tilting stiffness with respect to angular displacement of the bearing.

$$\boldsymbol{K} = \begin{bmatrix} 0.2901\text{N/mm} & -0.0002\text{N/mm} & -0.0272\text{N/mm} & 0.0291\text{N/rad} & -3.2776\text{N/rad} \\ -0.0002\text{N/mm} & 0.2662\text{N/mm} & 0.0007\text{N/mm} & 4.3096\text{N/rad} & -0.0291\text{N/rad} \\ -0.0272\text{N/mm} & 0.0007\text{N/mm} & 0.0210\text{N/mm} & 0.0097\text{N/rad} & -0.9277\text{N/rad} \\ 0.0291\text{N} & 4.3096\text{N} & 0.0097\text{N} & 423.20\text{Nmm/rad} & 0.2912\text{Nmm/rad} \\ -3.2776\text{N} & -0.0291\text{N} & -0.9277\text{N} & 0.2912\text{Nmm/rad} & 461.08\text{Nmm/rad} \end{bmatrix} \times 10^7 \tag{33}$$

Equation (33) shows that the tilting stiffness is far greater than the stiffness in other directions. This is mainly because the relative rotation of x axis and y axis occurs between the inner and outer rings of the double-row roller, and the radial and axial components of the contact force between the roller and the outer ring cause a resistance moment around the center of the bearing, which is related to the structure of the DRTRBs.

Figure 10 shows the relationship between the hub bearing stiffness and the vertical load on the ground. When the bearing is only subjected to the vertical load, the stiffness of the bearing along the x axis and y axis is much greater than the stiffness along the z axis; that is, the radial stiffness of the bearing is much larger than the axial stiffness, and the relationship between the stiffness magnitudes is $Kx>Ky>Kz$. The stiffness around the y axis is slightly greater than that around the x axis because the vertical load of the drive wheel induces the moment around the y axis. When the vertical load on the ground is less than 2000N, with the increase of the vertical load on the ground, the bearing stiffness shows a significant nonlinear increase. When the vertical load is small, the bearing stiffness increases rapidly, and as the load continues to increase, the increased amplitude of bearing stiffness decreases gradually. When the vertical load exceeds 2000N, the bearing stiffness increases linearly with the increase of the vertical load. The vertical load variation on one wheel of the light passenger car studied in this paper ranges from 4000N to 8000N (no load to full load), and the bearing stiffness is basically within the linear variation range.

Figure 11 shows the relationship between the diagonal element of the bearing stiffness matrix and the wheel driving torque when the hub bearing is only subjected to the driving torque. The radial stiffness of the bearing is much larger than the axial stiffness, which is consistent with the bearing stiffness under the vertical load. The relationship between the magnitudes of radial stiffness and axial stiffness is $Ky > Kx > Kz$. The bearing stiffness around the x axis is significantly greater than the bearing stiffness around the y axis. This is because the ground driving torque acting on the wheel causes the bearing to generate a torque around the x axis, so the stiffness around the x axis is larger. When the driving torque of the wheel is less than 200Nm, the bearing stiffness increases nonlinearly with the increase of the driving torque, and the increasing amplitude of bearing stiffness gradually decreases. When the driving torque exceeds 200 Nm, the diagonal element of the bearing stiffness matrix increases linearly with the increase of the driving torque.

7. Conclusions

In this paper, the stiffness matrix expression of double-row tapered roller hub bearings is derived, and the stiffness matrix is calculated by improved Newton-Raphson method. The conclusions are as follows:

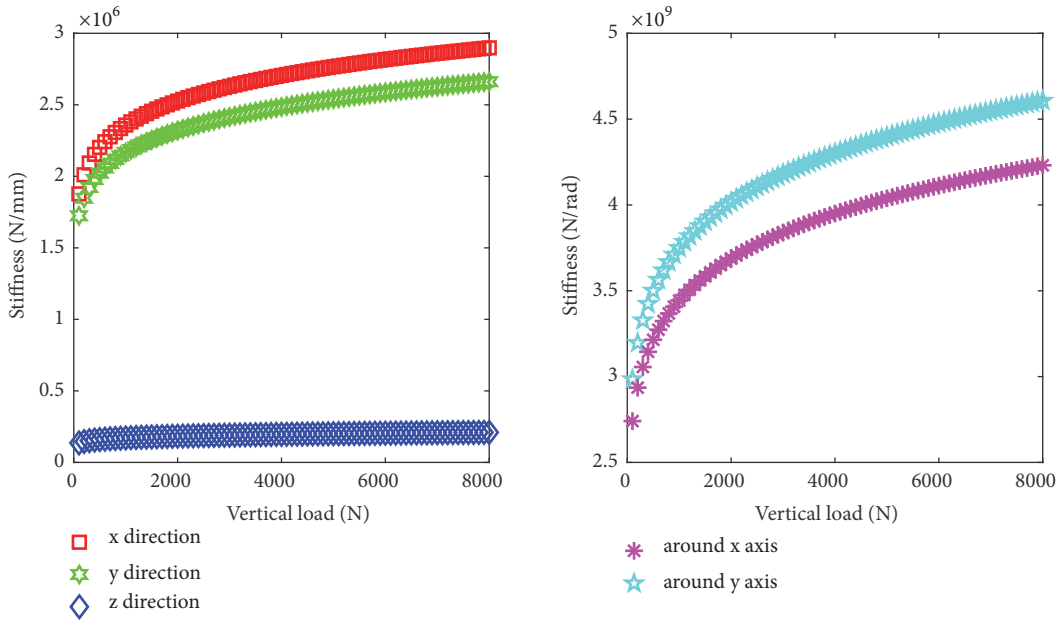

Figure 10: Relationship between hub bearing stiffness and vertical load.

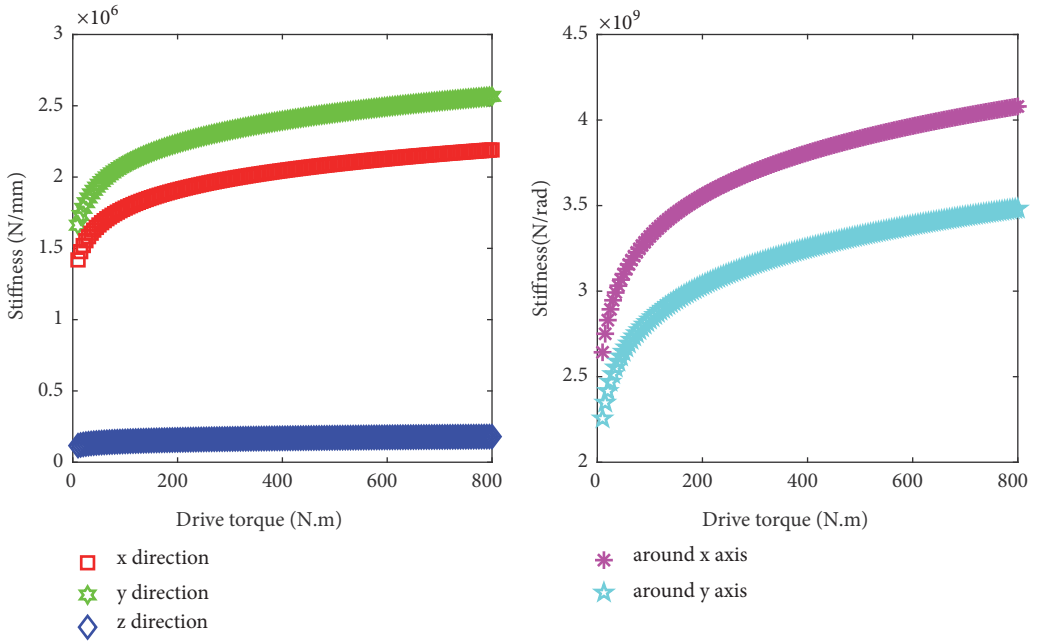

Figure 11: Relationship between hub bearing stiffness and wheel driving torque.

(1) The forces acting on the left rollers and the right rollers of DRTRBs are different. When calculating the overall stiffness of the hub bearing, the force acting on each roller should be considered separately.

(2) If the displacement between the inner ring and outer ring has been determined, the stiffness of the hub bearing can be directly calculated. If only the external loads of the hub bearing have been determined, the displacement of the hub bearing should be calculated by numerical method, and then the stiffness of the hub bearing should be calculated.

(3) The torsional stiffness of hub bearings around x axis and y axis is far greater than the stiffness in other directions. The radial stiffness of the hub bearing is much larger than the axial stiffness.

(4) Affected by vertical load on the ground and wheel drive torque, the stiffness of the hub bearing exhibits significant nonlinearity. The smaller the vertical ground load and wheel driving torque, the greater the influence of vertical ground load and wheel driving torque on the hub bearing stiffness.

Data Availability

Climate and demand data used to support the findings of this study are available from the first author upon request.

Conflicts of Interest

The authors declared no potential conflicts of interest with respect to the research, authorship, and/or publication of this article.

Acknowledgments

The research work was supported by National Key R&D Program of China (Grant no. 2018YFB0106203).

References

[1] R. Lostado, R. Escribano García, and R. Fernandez Martinez, "Optimization of operating conditions for a double-row tapered roller bearing," *International Journal of Mechanics and Materials in Design*, vol. 12, no. 3, pp. 353–373, 2016.

[2] R. Fernandez Martinez, R. Lostado Lorza, A. A. Santos Delgado, and N. O. Piedra Pullaguari, "Optimizing presetting attributes by softcomputing techniques to improve tapered roller bearings working conditions," *Advances in Engineering Software*, vol. 123, pp. 13–24, 2018.

[3] T. C. Lim and R. Singh, "Vibration transmission through rolling element bearings, part I: bearing stiffness formulation," *Journal of Sound and Vibration*, vol. 139, no. 2, pp. 179–199, 1990.

[4] V.-C. Tong and S.-W. Hong, "Characteristics of tapered roller bearing subjected to combined radial and moment loads," *International Journal of Precision Engineering and Manufacturing - Green Technology*, vol. 1, no. 4, pp. 323–328, 2014.

[5] R. J. Lambert, A. Pollard, and B. J. Stone, "Some characteristics of rolling-element bearings under oscillating conditions. Part 2: Experimental results for interference-fitted taper-roller bearings," *Proceedings of the Institution of Mechanical Engineers, Part K: Journal of Multi-body Dynamics*, vol. 220, no. 3, pp. 171–179, 2006.

[6] R. J. Lambert, A. Pollard, and B. J. Stone, "Some characteristics of rolling-element bearings under oscillating conditions. Part 3: Experimental results for clearance-fitted taper-roller bearings and their relevance to the design of spindles with high dynamic stiffness," *Proceedings of the Institution of Mechanical Engineers, Part K: Journal of Multi-body Dynamics*, vol. 220, no. 3, pp. 181–190, 2006.

[7] V. Tong and S. Hong, "Optimization of partially crowned roller profiles for tapered roller bearings," *Journal of Mechanical Science and Technology*, vol. 31, no. 2, pp. 641–650, 2017.

[8] M. F. While, "Rolling element bearing vibration transfer characteristics: effect of stiffness," *Journal of Applied Mechanics*, vol. 46, no. 3, pp. 677–684, 1979.

[9] T. Lim and R. Singh, "Vibration transmission through rolling element bearings, part V: effect of distributed contact load on roller bearing stiffness matrix," *Journal of Sound and Vibration*, vol. 169, no. 4, pp. 547–553, 1994.

[10] H.-V. Liew and T. C. Lim, "Analysis of time-varying rolling element bearing characteristics," *Journal of Sound and Vibration*, vol. 283, no. 3–5, pp. 1163–1179, 2005.

[11] A. Palmgren, *Ball and Roller Bearing Engineering*, Philadelphia, Burbank, 1959.

[12] A. B. Jones, "A general theory for elastically constrained ball and radial roller bearings under arbitrary load and speed conditions," *Journal of Fluids Engineering*, vol. 82, no. 2, pp. 309–320, 1960.

[13] D. Dowson and G. R. Higginson, "Theory of roller-bearing lubrication and deformation," *Wear*, vol. 6, no. 6, article no 496, 1963.

[14] T. A. Harris, *Rolling Bearing Analysis*, Wiley, New York, 1984.

[15] M. D. Rajab, *Modeling of the Transmissibility Through Rolling Element Bearing under Radial and Moment Loads*, PhD Dissertation, The Ohio State University, 1982.

[16] W. B. Young, *Dynamics Modeling and Experimental Measurement of a Gear Shaft and Housing System, MS Thesis*, The Ohio State University, 1988.

[17] J. M. de Mul, J. M. Vree, and D. A. Maas, "Equilibrium and associated load distribution in ball and roller bearings loaded in five degrees of freedom while neglecting friction—part I: general theory and application to ball bearings," *Journal of Tribology*, vol. 111, no. 1, pp. 142–148, 1989.

[18] J. M. de Mul, J. M. Vree, and D. A. Maas, "Equilibrium and associated load distribution in ball and roller bearings loaded in five degrees of freedom while neglecting friction—part II: application to roller bearings and experimental verification," *Journal of Tribology*, vol. 111, no. 1, pp. 149–155, 1989.

[19] V. Tong and S. Hong, "Study on the stiffness and fatigue life of tapered roller bearings with roller diameter error," *Proceedings of the Institution of Mechanical Engineers, Part J: Journal of Engineering Tribology*, vol. 231, no. 2, pp. 176–188, 2016.

[20] S. Kabus, M. R. Hansen, and O. Ø. Mouritsen, "A new quasi-static multi-degree of freedom tapered roller bearing model to accurately consider non-Hertzian contact pressures in time-domain simulations," *Proceedings of the Institution of Mechanical Engineers, Part K: Journal of Multi-body Dynamics*, vol. 228, no. 2, pp. 111–125, 2014.

[21] A. Bourdon, J. F. Rigal, and D. Play, "Static rolling bearing models in a C.A.D. environment for the study of complex mechanisms: part i—rolling bearing model," *Journal of Tribology*, vol. 121, no. 2, p. 205, 1999.

[22] Y. Guo and R. G. Parker, "Stiffness matrix calculation of rolling element bearings using a finite element/contact mechanics model," *Mechanism and Machine Theory*, vol. 51, pp. 32–45, 2012.

[23] A. Gunduz and R. Singh, "Stiffness matrix formulation for double row angular contact ball bearings: Analytical development and validation," *Journal of Sound and Vibration*, vol. 332, no. 22, pp. 5898–5916, 2013.

[24] I. Bercea, S. Cretu, and D. Nélias, "Analysis of double-row tapered roller bearings, part I - model," *Tribology Transactions*, vol. 46, no. 2, pp. 228–239, 2003.

[25] D. Nélias, I. Bercea, and N. Mitu, "Analysis of double-row tapered roller bearings, part II – results: prediction of fatigue life and heat dissipation," *Tribology Transactions*, vol. 46, no. 2, pp. 240–247, 2003.

[26] I. Bercea, D. Nélias, and G. Cavallaro, "A unified and simplified treatment of the non-linear equilibrium problem of double-row rolling bearings. Part 1: Rolling bearing model," *Proceedings of the Institution of Mechanical Engineers, Part J: Journal of Engineering Tribology*, vol. 217, no. 3, pp. 205–212, 2005.

[27] J. Brändlein, P. Eschmann, L. Hasbargen et al., *Ball and Roller Bearings: Theory, Design, and Application*, John Wiley & Sons, Ltd, 3rd edition, 1999.

[28] H. Sjovall, "Belastningsfordelningen inom kul-och rullager vid givna yttre radial-och axialbelastningar," *Teknisk Tidskrifr. Mekanik*, 1933.

[29] L. Houpert, "A Uniform analytical approach for ball and roller bearings calculations," *Journal of Tribology*, vol. 119, no. 4, pp. 851–858, 1997.

[30] D. Changan, Z. Lei, and Z. Fuzhang, "Theoretical formula for calculation of line-contact elastic contact deformation," *Journal of Tribology*, vol. 21, no. 2, pp. 135–138, 2001.

[31] W. Hao, *Research on The Dynamic Characteristics of Rolling Element Bearings and The Dynamic Model of Bearing Rotor System*, East China University of Science and Technology, 2012.

[32] L. Jiwei and L. Tianyu, *Analysis, Calculation and Application of Rolling Bearing*, Machinery Industry Press, 2009.

[33] P. Göncz, M. Ulbin, and S. Glodež, "Computational assessment of the allowable static contact loading of a roller-slewing bearing's case-hardened raceway," *International Journal of Mechanical Sciences*, vol. 94-95, pp. 174–184, 2015.

[34] K. Fallahnezhad, S. Liu, O. Brinji, M. Marker, and P. A. Meehan, "Monitoring and modelling of false brinelling for railway bearings," *Wear*, vol. 424-425, pp. 151–164, 2019.

[35] N. Demirhan and B. Kanber, "Stress and displacement distributions on cylindrical roller bearing rings using FEM," *Mechanics Based Design of Structures and Machines*, vol. 36, no. 1, pp. 86–102, 2008.

[36] T. A. Harris and M. N. Kotzalas, *Essential Concepts of Bearing Technology: Rolling Bearing Analysis*, CRC press, New York, NY, USA, 2006.

[37] L. Kania, "Modelling of rollers in calculation of slewing bearing with the use of finite elements," *Mechanism and Machine Theory*, vol. 41, no. 11, pp. 1359–1376, 2006.